Journal of Materials Chemistry B

PAPER

View Article Online
View Journal | View Issue

Published on 06 August 2014. Downloaded by University of Illinois at Chicago on 28/10/2014 13:00:31.

Cite this: J. Mater. Chem. B, 2014, 2, 6626

Mn^{2+}-doped $NaYF_4$:Yb/Er upconversion nanoparticles with amplified electrogenerated chemiluminescence for tumor biomarker detection

Min Liu,[a] Yuhang Ye,[a] Cheng Yao,[b] Wenbo Zhao*[a] and Xiaohua Huang*[a]

Received 5th May 2014
Accepted 6th August 2014

DOI: 10.1039/c4tb00717d

www.rsc.org/MaterialsB

Chemiluminescence was used as an excitation light source to construct a universal photoelectrochemical platform based on Mn^{2+}-doped $NaYF_4$:Yb/Er upconversion nanoparticles, which greatly improves the electrochemiluminescence intensity and offers more stable cathodic signals compared to pure $NaYF_4$:Yb/Er NPs. Here, we report for the first time the ECL behaviors of Mn^{2+}-doped $NaYF_4$:Yb/Er NPs, which were synthesized *via* a facile strategy. Mn^{2+} doping resulted in a 4-fold ECL intensity enhancement of $NaYF_4$:Yb/Er. The characteristics of Mn^{2+}-doped $NaYF_4$:Yb/Er nanocomposites were obtained using transmission electron microscopy (TEM), energy dispersive X-ray spectrometer (EDS), and fluorescence spectra. After all the results had indicated that $NaYF_4$:Yb/Er upconversion nanoparticles were successfully doped with Mn^{2+}, the electrochemiluminescence platform was built. The as-prepared $NaYF_4$:Yb/Er NPs were rendered water-soluble and then employed as ECL emitters for carcinoembryonic antigen (CEA) determination. The results indicated that the modified electrode can be used to determine CEA without interference from non-specific proteins, with a low detection limit of 5.2 pg mL^{-1}. The biosensor can also be used for quantification of the CEA concentration in real samples.

1. Introduction

Recent decades have witnessed an explosion in research devoted to electrogenerated chemiluminescence (electrochemiluminescence, ECL), which intrinsically represents a marriage between electrochemistry and spectroscopy.[1–4] By integrating the advantages of both, ECL possesses unique superiorities over other optical methods. It does not require a light source, which not only simplifies the detection apparatus but also invalidates background signals from scattered light and luminescent impurities, thus leading to high sensitivity.[5] The ECL technique has also become a powerful analytical tool in biomolecule detection, clinical diagnostics, environmental and food monitoring, biowarfare agent detection, *etc.*[6–10] ECL emitters are continuously evolving, and the advances that have occurred regarding nanoparticle (NP)-based ECL not only open a promising field for the development of next-generation ECL-emitting species, but also complement the conventional optical utilization of quantum dots (QDs).[11–13]

Rare earth-doped upconversion nanoparticles (UCNPs) possess many advantages, such as narrow emission peak, long fluorescence lifetime, high photochemical stability, large Stokes shift, and low toxicity.[14–16] As a new ECL emitter, UCNPs have attracted wide interest. In the past decades, great efforts have been dedicated to QD-based ECL, which has been widely applied in biosensing and bioanalysis.[17] Compared with QDs, rare earth-doped luminescent nanoparticles have been proposed as a promising new class of ECL emitters because of their attractive chemical and optical features,[18–20] including low toxicity, considerable ECL intensity, and stable cathodic signals. Doped nanocrystal (NC) materials possessing special ECL properties are extremely desirable for the analysis of a great variety of biomolecules.[21] Xu *et al.* successfully demonstrated that manganese ion (Mn^{2+})-doped ZnS:Mn NCs generate a new cathodic ECL emission peak at much more positive potential,[22] and that spin-dependent energy transfer between the doped Mn^{2+} ions and host CdS NCs also exists in the ECL emission process of CdS:Mn NCs.[23] In the photoluminescence (PL) field, it was proven that the pure far red emission (650–670 nm) of $NaYF_4$:Yb/Er NPs was achieved by Mn^{2+} doping;[24] however, the applications of Mn^{2+}-doped $NaYF_4$:Yb/Er NPs in ECL fields still remain unexplored.

Carcinoembryonic antigen (CEA), an acidic glycoprotein with a molecular weight of approximately 200 kDa, is recognized as the most commonly used tumor marker in clinical cancer screening and early diagnostic applications.[25–29] Therefore, sensitive, precise, and accurate assays for the

[a]Jiangsu Key Laboratory of Biofunctional Materials, College of Chemistry and Materials Science, Nanjing Normal University, Nanjing 210023, P. R. China. E-mail: zhaowenbo@njnu.edu.cn; xiaohuahuang_njnu@163.com; Fax: +86-25-83598280; +86 25 83598280; Tel: +86-25-85891651; +86 25 85891536

[b]State Key Laboratory of Materials-Oriented Chemical Engineering and College of Science, Nanjing University of Technology, Nanjing 210009, P. R. China. Fax: +86-25-8358-7433

This journal is © The Royal Society of Chemistry 2014

Published on 06 August 2014. Downloaded by University of Illinois at Chicago on 28/10/2014 13:00:31.

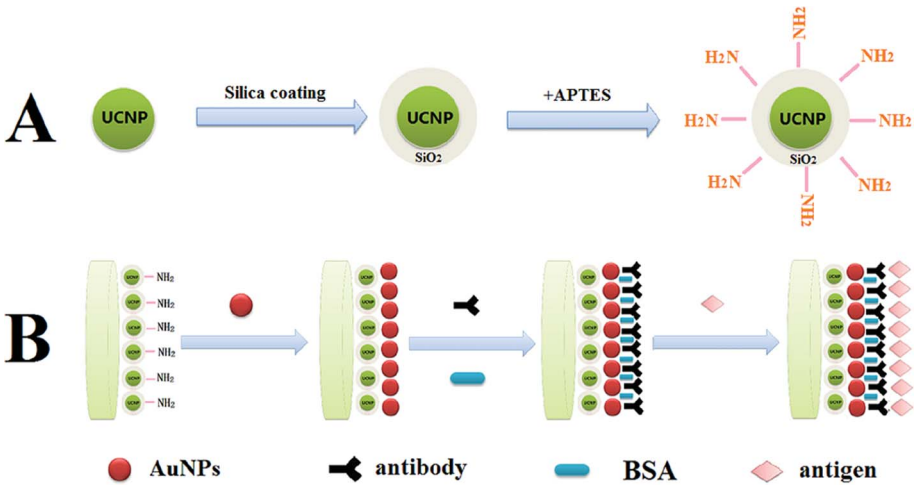

Scheme 1 Schematic representation of ECL immunosensor preparation.

determination of low concentrations of CEA in complex biological samples are necessary. Immunoassays are based on the use of an antibody that specifically reacts with an antigen to be tested,[30] which is a powerful analytical tool for CEA determination. Herein, an electrogenerated chemiluminescence immunosensor based on Mn^{2+}-doped $NaYF_4$:Yb/Er upconversion NPs for sensitive detection of a tumor marker is described (Scheme 1).

In this work, we report the ECL behaviors of Mn^{2+}-doped $NaYF_4$:Yb/Er NPs for the first time. Mn^{2+}-doped $NaYF_4$:Yb/Er NPs were synthesized *via* a facile strategy, and 4-fold ECL intensity enhancement of $NaYF_4$:Yb/Er UCNPs was achieved by Mn^{2+} doping. The existence of Mn^{2+} ions disturbed the energy transfer between green and red emissions of Er^{3+} and facilitated the occurrence of red emission, generating a high-intensity ECL signal with satisfactory stability. Moreover, the Mn^{2+} doping also influenced the growth dynamics so that simultaneous control of the crystalline phase and size of the resulting UCNPs was obtained. By coating a layer of silica on the surface of the NPs, the as-prepared UCNPs were rendered water-soluble and then employed as ECL emitters for CEA determination.

2. Experimental section

2.1. Materials

$MnCl_2 \cdot 4H_2O$, $Y(NO_3)_3 \cdot 6H_2O$, $Yb(NO_3)_3 \cdot 6H_2O$, $Er(NO_3)_3 \cdot 6H_2O$, bovine serum albumin (BSA), sodium citrate, and glucose were purchased from Aladdin Reagent Co., China. Oleic acid (technical grade, 90%), uric acid (UA), and ascorbic acid (AA) were all supplied by Alfa Aesar Reagent Company and used without further purification. Tetraethyl orthosilicate (TEOS), ethanol, cyclohexane, isopropanol, chloroform, NaOH, and NaF were of analytical reagent grade and used as received. Gold chloride ($HAuCl_4 \cdot 4H_2O$) was obtained from Sigma Chemical Co., China. Aqueous ammonia solution (NH_4OH, 71 wt% water, 29 wt% ammonia) was obtained from Shanghai Lingfeng Chemical Co. Ltd., China. Organosilanes (3-aminopropyl)triethoxysilane (APTES) was purchased from GELEST Inc., USA. CEA standard solutions were obtained from enzyme-linked immunosorbent assay (ELISA) kits for CEA. ATP and anti-CEA (Ab) were purchased from Zhengzhou Biocell Co., China and stored at 4 °C before use.

2.2. Instrumentation

Transmission electron microscopy (TEM) images were obtained using an interface high-resolution transmission electron microscope (Hitachi H-7650, Japan). The elemental content was analyzed with an energy dispersive X-ray spectrometer (EDS, JSM-5610LV/NORAN-VANTAGE). Fluorescence spectra were recorded on a Perkin-Elmer LS 50B fluorescence spectrophotometer at room temperature. Fourier transform infrared (FTIR) spectra were obtained in the range of 3900–500 cm^{-1} with a NEXUS 670 (Nicolet) FTIR instrument. The X-ray diffraction (XRD) pattern was recorded on a powder sample using a D/max 2500VL/PC diffractometer (Japan) equipped with graphite monochromatized Cu Kα radiation (λ = 1.54060 Å) in 2θ ranging from 10° to 90°. The ECL emission was detected with an MPI-E electrochemiluminescence analyzer (Xi'An Remax Electronic Science & Technology Co. Ltd., Xi'An, China). All electrochemical experiments were performed on a CHI760C electrochemical analyzer (CH Instruments, Inc., US) using a conventional three-electrode system with a glassy carbon electrode (GCE, 3 mm in diameter, Shanghai Chenhua, China) as the working electrode, a platinum wire as the auxiliary electrode, and a saturated calomel electrode (SCE) as the reference electrode. Electrochemical impedance measurements were performed in 0.1 M KCl solution containing 5 mM $Fe(CN)_6^{3-/4-}$ (1 : 1) and plotted in the form of complex plane diagrams (Nyquist plots).

2.3. Preparation of upconversion nanoparticles (UCNPs) and water-soluble UCNPs

The preparation process of UCNPs has been previously described.[24] Pure $NaYF_4$:Yb/Er nanocrystals and Mn^{2+}-ion doped $NaYF_4$:Yb/Er nanocrystals were prepared by varying the

Published on 06 August 2014. Downloaded by University of Illinois at Chicago on 28/10/2014 13:00:31.

value of x ("x" is the volume of the 0.5 M Mn^{2+} ion solution used, $0 \leq x \leq 0.6$) in the reaction system. X mL of 0.5 M $MnCl_2$, $(1.6 - x)$ mL of 0.5 M $Y(NO_3)_3$, 0.9 mL of 0.2 M $Yb(NO_3)_3$, and 0.1 mL of 0.2 M $Er(NO_3)_3$ were added to a mixture of NaOH (0.3 g), deionized water (1.5 mL), oleic acid (5 mL) and ethanol (10 mL) under continuous stirring. 2 mL of deionized water containing 4 mmol of NaF was then added dropwise to the mixture. After vigorous stirring at room temperature for 15 min, the colloidal solution was transferred into a 25 mL Teflon-lined autoclave, sealed, and heated at 200 °C for 8 h. The solutions were then allowed to naturally cool to room temperature. The final products were collected by centrifugation, washed with ethanol and deionized water several times to remove any possible remnants, and then dried in vacuum at 70 °C to obtain the dried UCNP powder. The core–shell-structured Mn^{2+}-$NaYF_4$:Yb/Er@SiO_2 NPs were prepared by a modified Stöber sol–gel process (Scheme 1A).[31] Typically, 30 mg of Mn^{2+}-$NaYF_4$:Yb/Er NPs was dispersed in 80 mL of isopropyl alcohol by sonication for 1 h. Then 7.5 mL of deionized water and 54 μL of TEOS were added, followed by titration with 8.94 mL of ammonium hydroxide. The reaction was carried out with vigorous stirring at room temperature for 4 h, and then 26 μL of APTES was added and allowed to react for another 1 h, yielding amino-modified core–shell-structured $NaYF_4$:Yb/Er@SiO_2 NPs. These Mn^{2+}-$NaYF_4$:Yb/Er@SiO_2–NH_2 NPs could be redispersed in deionized water for further use.

2.4. Fabrication of the as-prepared immunosensor

The glassy carbon electrode was polished with 0.3 and 0.05 μm alumina slurry and then sonicated in ethanol and double-distilled water for 5 min each. After that, the GCE was allowed to dry at room temperature to form a mirror-like surface. To prepare the modified electrode, firstly, 10.0 μL of the obtained Mn^{2+}-$NaYF_4$:Yb/Er@SiO_2–NH_2 NP solution was dropped onto the electrode surface and dried in air. Then, 10.0 μL of Au colloid was dropped onto the surface of (Mn^{2+}-$NaYF_4$:Yb/Er@SiO_2–NH_2 NPs)/GCE, and then the electrode was dipped into a solution of anti-CEA (0.1 mg mL^{-1} in 0.1 M phosphate buffer solution (PBS), pH 7.4) overnight at 4 °C to absorb the antibodies. Finally, the modified immunosensor was incubated in a solution of BSA (1%, w/w) for approximately 1 h. The immunosensor was stored at 4 °C.

3. Results and discussion

3.1. Characterization of the Mn^{2+}-doped $NaYF_4$:Yb/Er upconversion nanoparticles (UCNPs) and water-soluble UCNPs

The Mn^{2+}-doped $NaYF_4$:Yb/Er (18/2 mol%) NPs were prepared by a modified liquid-solid-solution (LSS) solvothermal route first reported by Li *et al.*[32] The shape, phase, and composition of $NaYF_4$ NPs doped with Mn^{2+} were studied by transmission electron microscopy (TEM), X-ray diffraction (XRD), and energy dispersive X-ray spectrometry (EDS). As shown in Fig. 1A, two distinct particle morphologies that include small nanocubes (cubic phase) and larger hexagonal nanorods (hexagonal phase)

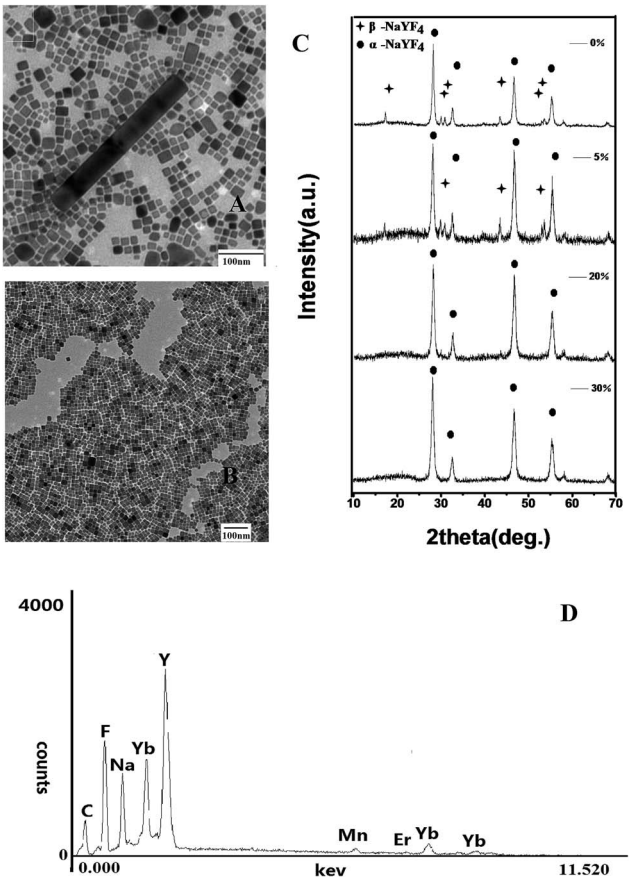

Fig. 1 TEM images of NaYF4:Yb/Er (18/2 mol%) nanocrystals (A) without Mn^{2+} dopant ions and (B) with 30 mol% Mn^{2+} dopant ions. (C) X-ray powder diffraction patterns of $NaYF_4$:Yb/Er (18/2 mol%) in the presence of 0, 5, 20, and 30 mol% Mn^{2+} dopant ions. (D) Typical EDS spectra taken of 30 mol% Mn^{2+}-$NaYF_4$:Yb/Er.

were observed. With addition of 30 mol% Mn^{2+}, the $NaYF_4$ nanocrystals turned into well-crystallized nanocubes with a uniform size of 15–20 nm (Fig. 1B). Upon doping with increasing concentrations of Mn^{2+} ions, the phase transformation from hexagonal to cubic was obvious and was verified by XRD analysis (Fig. 1C). The XRD patterns of the pure and 5 mol% Mn^{2+}-doped samples are indexed to the mixture of the hexagonal (JCPDS file number 16-334) and cubic phase (JCPDS file number 6-342), respectively. Remarkably, when 20 mol% and 30 mol% Mn^{2+} doping was used, all the XRD peaks matched well with those of the cubic $NaYF_4$ phase (JCPDS file number 6-342), and no obvious extra diffraction peaks were detected. EDS measurements of the Mn^{2+}-doped $NaYF_4$:Yb/Er structure revealed its composition (Fig. 1D). As could be seen from Fig. 1D, a clear peak belonged to Mn, which confirmed the successful synthesis of Mn^{2+}-doped $NaYF_4$:Yb/Er.

Mn^{2+} doping not only facilitates the output of red emission but also enhances the intensity of UCNP emission. The introduction of sufficient Mn^{2+} ions into $NaYF_4$:Yb/Er leads to a brilliant red emission (Fig. 2), which is as much as 8 times brighter than that of a Mn-free sample. To verify the efficiency of Mn^{2+}-doped $NaYF_4$:Yb/Er, we first investigated the ECL signal

 This journal is © The Royal Society of Chemistry 2014

Published on 06 August 2014. Downloaded by University of Illinois at Chicago on 28/10/2014 13:00:31.

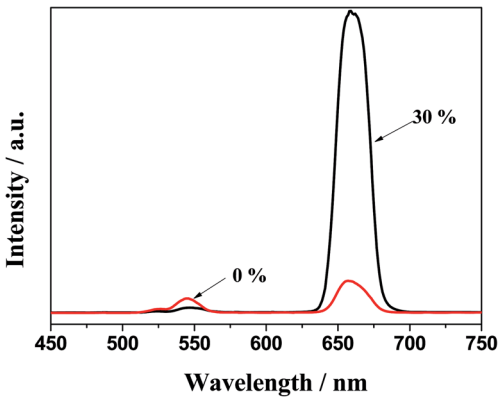

Fig. 2 Upconversion emission spectra of NaYF4:Yb/Er (18/2 mol%) nanocrystals with 0 and 30 mol% Mn^{2+} dopant ions dispersed in cyclohexane (1 mg mL^{-1}).

and the stability of the nanomaterial-modified electrode. Similarly, $NaYF_4$:Yb/Er NCs doped with Mn^{2+} ions had a great effect on the ECL intensity (Fig. 3A). The ECL intensity reached a maximum at 30% doping, resulting in a 4-fold ECL enhancement compared to pure $NaYF_4$:Yb/Er NCs. Furthermore, the 30% Mn^{2+}-doped $NaYF_4$:Yb/Er nanocomposites also exhibited an excellent ECL emission stability. As shown in Fig. 3B, stable and intense ECL signals of Mn^{2+}-$NaYF_4$:Yb/Er NPs (30%) were observed under continuous potential scanning. No obvious change in the ECL intensity of the Mn^{2+}-$NaYF_4$:Yb/Er NPs (30%) was observed after storage for half a year. This result indicated that Mn^{2+}-$NaYF_4$:Yb/Er film is a perfect platform to construct ECL-based biosensors.

In the presence of co-reactant $S_2O_8^{2-}$ ions, the ECL processes of the as-prepared Mn^{2+}-$NaYF_4$:Yb/Er film are proposed as follows:

$$Mn^{2+}\text{-}NaYF_4\text{:Yb/Er} + ne^- \rightarrow n(Mn^{2+}\text{-}NaYF_4\text{:Yb/Er})^{-\cdot} \quad (1)$$

$$S_2O_8^{2-} + e^- \rightarrow SO_4^{2-} + SO_4^{-\cdot} \quad (2)$$

$$(Mn^{2+}\text{-}NaYF_4\text{:Yb/Er})^{-\cdot} + SO_4^{-\cdot} \rightarrow (Mn^{2+}\text{-}NaYF_4\text{:Yb/Er})^* + SO_4^{2-} \quad (3)$$

$$(Mn^{2+}\text{-}NaYF_4\text{:Yb/Er})^* \rightarrow Mn^{2+}\text{-}NaYF_4\text{:Yb/Er} + h\nu \quad (4)$$

To create water-dispersible NCs that are suitable for conjugation, a uniform SiO_2–NH_2 layer was coated on their surface using a microemulsion method.[33] Fig. 4A shows a typical TEM image of the SiO_2–NH_2 layers coated on Mn^{2+}-$NaYF_4$:Yb/Er NCs with an average diameter of 40 nm. These NCs are uniform in size and hydrophilic due to the capping of the silica layer on their surface. The layer consists of amorphous SiO_2 with a

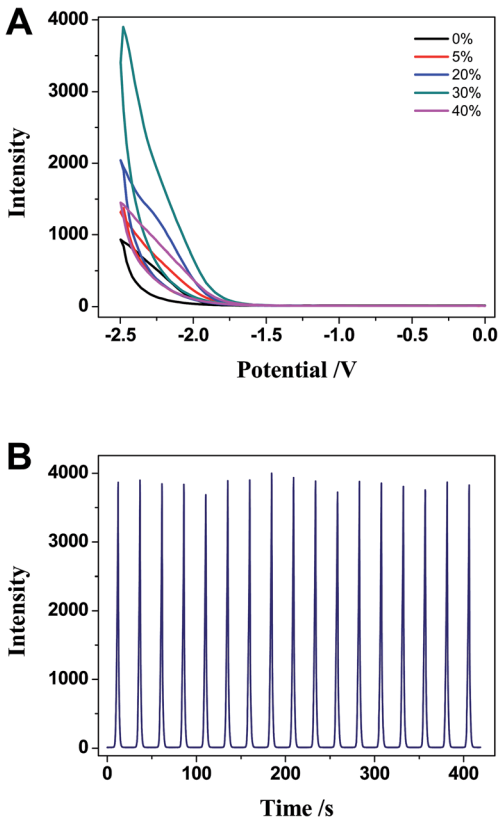

Fig. 3 (A) Cyclic ECL curves of the dependence of ECL emission on the Mn^{2+} doping level in $NaYF_4$:Yb/Er NPs. (B) ECL behaviors of Mn^{2+}-$NaYF_4$:Yb/Er NPs (30%) in 0.10 M, pH 7.4 PBS containing 0.1 M $K_2S_2O_8$. The potential was scanned in the negative direction from 0 to −2.5 V with a scan rate of 100 mV s^{-1}.

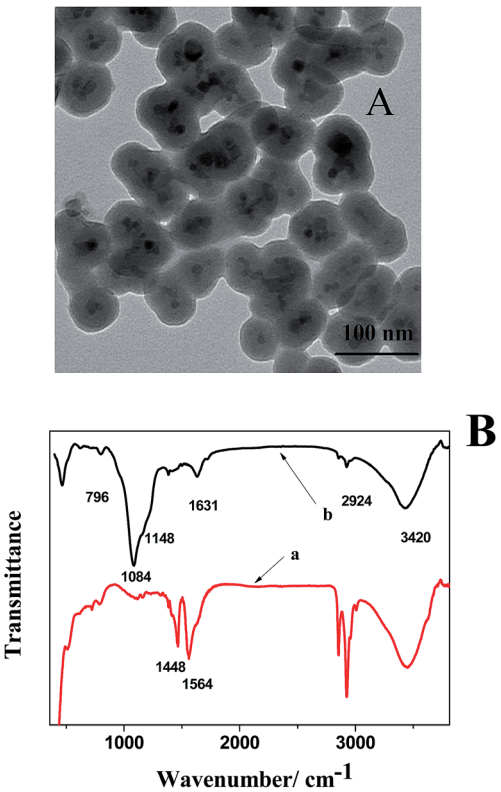

Fig. 4 (A) TEM images of prepared Mn^{2+}-$NaYF_4$:Yb/Er nanocrystals after coating with a 10 nm SiO_2–NH_2 layer. (B) FTIR of prepared $NaYF_4$:Yb/Er nanocrystals before (a) and after (b) coating with a 10 nm SiO_2–NH_2 layer.

Published on 06 August 2014. Downloaded by University of Illinois at Chicago on 28/10/2014 13:00:31.

thickness of approximately 10 nm, as shown in the TEM image. After the amino modification process, the FTIR spectra were used to characterize the functionalization of $NaYF_4$:Yb/Er NPs with silica and $-NH_2$ groups. Fig. 4B shows the FTIR spectra of the capping ligands on the surface of Mn^{2+}-$NaYF_4$:Yb/Er NPs and Mn^{2+}-$NaYF_4$:Yb/Er NPs functionalized with SiO_2–NH_2 layers. Bands at 1564 and 1448 cm^{-1} were found in the spectrum of the Mn^{2+}-$NaYF_4$:Yb/Er sample, associated with the asymmetric and symmetric stretching vibrations of the carboxylic group of the bound oleic acid. The results indicated that the as-formed Mn^{2+}-$NaYF_4$:Yb/Er NPs were coated by oleic acid.

After the reaction of Mn^{2+}-$NaYF_4$:Yb/Er NPs with (3-aminopropyl)triethoxysilane (APTES) and tetraethyl orthosilicate (TEOS) in NH_4OH aqueous solution, the FTIR spectrum showed a broad absorption peak at 3420 cm^{-1} that was due to the asymmetric stretching vibration of the primary amino group ($-NH_2$). It became weaker than that of –OH absorption near the same region. The two absorption peaks at 1631 and 796 cm^{-1} are due to the scissoring and wagging vibrations of the $-NH_2$ groups, respectively. The two strong absorption peaks at 1148 and 1084 cm^{-1} resulted from the Si–O–Si asymmetric vibration. The weak peak at 2924 cm^{-1} is due to the asymmetrical stretching vibration modes of the $-CH_2$ groups. From these results, it can be confirmed that after the functionalization reaction with APTES and TEOS, the Mn^{2+}-$NaYF_4$:Yb/Er NPs had been covered with a silica layer containing functional $-NH_2$ groups on their surface due to the polycondensation process between TEOS and APTES. The amino groups on the Mn^{2+}-$NaYF_4$:Yb/Er@SiO_2 nanoparticles provide a powerful 'claw' to grab gold nanocrystals due to the strong coordination between the gold and the $-NH_2$ group.[34]

3.2. EIS of the immunosensor

Fig. 5 shows the Nyquist plots of electrochemical impedance resistance (EIS) observed upon the stepwise modification processes in 0.1 M PBS (5 mM $[Fe(CN)_6]^{3-/4-}$ + 0.1 M KCl, pH 7.4). The bare GCE revealed a small semicircle domain (Fig. 5a), which implies a low R_{et} value of the redox couple, *i.e.*, $[Fe(CN)_6]^{3-/4-}$. Due to its semiconductive properties, silica could restrain the electron transfer,[35] and it was observed that the EIS of (Mn^{2+}-$NaYF_4$:Yb/Er@SiO_2–NH_2)/GCE was larger than that of the bare electrode (Fig. 5b). After modification with Au NPs, the resulting electrode showed a much lower resistance, which implied that the conductive Au NPs can accelerate the electron transfer (Fig. 5c). It has been reported that the antigen–antibody complex could act as a layer that disturbs ion diffusion and alters electrical capacitance,[36] and both factors would significantly affect the electrochemical impedance of electrodes during the formation of antigen–antibody complex (Fig. 5d–f). These facts assisted with the completion of the electrode surface assembly process.

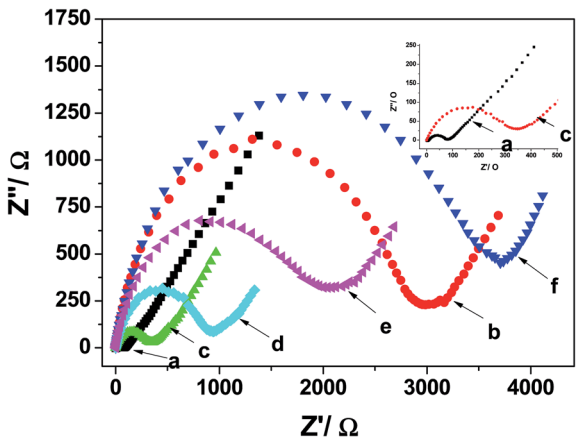

Fig. 5 EIS for each immobilized step in 0.1 M KCl solution containing 5 mM $[Fe(CN)_6]^{4-/3-}$: (a) GCE; (b) (Mn^{2+}-$NaYF_4$:Yb/Er@SiO_2–NH_2)/GCE; (c) Au NPs/(Mn^{2+}-$NaYF_4$:Yb/Er@SiO_2–NH_2)/GCE; (d) Ab/Au NPs/(Mn^{2+}-$NaYF_4$:Yb/Er@SiO_2–NH_2)/GCE; (e) BSA/Ab/Au NPs/(Mn^{2+}-$NaYF_4$:Yb/Er@SiO_2–NH_2)/GCE; (f) Ag/BSA/Ab/Au NPs/(Mn^{2+}-$NaYF_4$:Yb/Er@SiO_2–NH_2)/GCE.

3.3. Optimization of detection conditions

The sensitivity of the immunosensor is often related to factors such as pH values of the PBS, and incubation time.[37,38] These factors were optimized when the immunosensor was incubated in 10 ng mL^{-1} CEA. The effects of solution pH on the ECL signals to the CEA are shown in Fig. 6A. The ECL intensity increased with increasing pH values from 5.0 to 6.0 and then

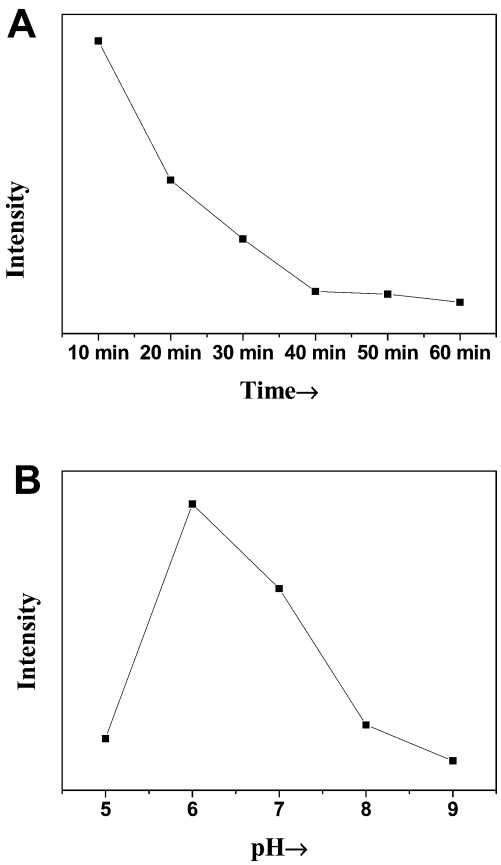

Fig. 6 Effects of (A) pH of detection solution, and (B) incubation time. One parameter was changed while the others were at their optimal conditions, and 10 ng mL^{-1} CEA was used as an example.

This journal is © The Royal Society of Chemistry 2014

Published on 06 August 2014. Downloaded by University of Illinois at Chicago on 28/10/2014 13:00:31.

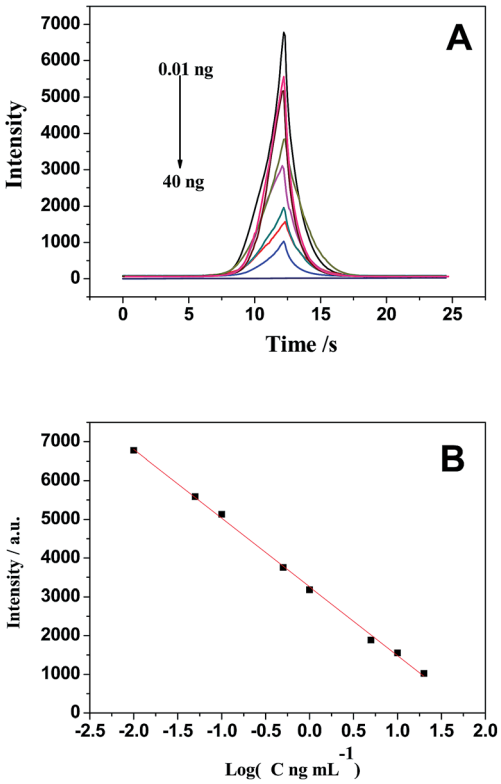

Fig. 7 (A) ECL curves of as-prepared electrode in different concentrations of CEA (0.01–20 ng mL^{-1}) in the negative direction from 0 to −2.5 V (*vs.* SCE) with a scan rate of 200 mV s^{-1}, (B) linear calibration curve for CEA determination in 0.10 M, pH 6.0 PBS containing 0.1 M $K_2S_2O_8$. The PMT was set at 700 V.

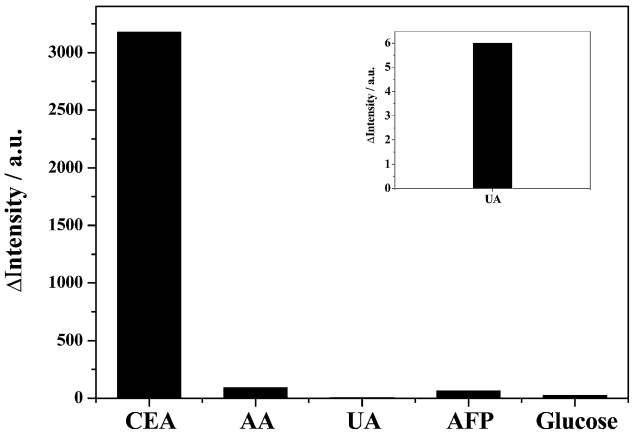

Fig. 8 The interfering effect of the samples on the ECL intensity of the immunosensors. The histogram represents the influence of nonspecific adsorption of CEA when the electrode was without anti-CEA. The concentration of all the samples was 1 ng mL^{-1}. (The inset shows the enlarged image of the UA effect on the ECL intensity of the immunosensors.)

decreased when the pH value was greater than 6.0. Thus, the PBS with pH 6.0 was selected for preparation of the detection solution. For the incubation time, the ECL signals to the CEA decreased with increasing incubation time and then started to level off at 40 min (Fig. 6B). Therefore, an incubation time of 40 min was selected for later assays.

3.4. Analytical performance

Under optimized conditions, the dose–response curve and the calibration curve for CEA immunoassay are shown in Fig. 7. The linear range for CEA detection was from 0.01 to 40 ng mL^{-1} with a relative coefficient of 0.996 and a detection limit of 5.2 pg mL^{-1} at 3 times the standard deviation of the blank response. The CEA detection performance of the proposed biosensor was compared with other methods. As shown in Table 1, (Mn^{2+}-$NaYF_4$:Yb/Er@SiO_2–NH_2)/GCE exhibited excellent performance in terms of a wider linear range and lower limit of detection for CEA. The sensitivity was also higher than those of gold nanolabel-enhanced ECL immunoassay methods.[39–41] When the ECL immunoassay was not being performed, the immunosensor could be stored in stock buffer at 4 °C for 2 weeks without any obvious signal change.

3.5. Selectivity of the immunosensor

In order to evaluate the selectivity of the developed immunosensor for CEA, the ECL intensity changes induced by interferences such as UA, glucose, AFP, and AA were measured. The selectivity of the novel Mn^{2+}-$NaYF_4$:Yb/Er@SiO_2–NH_2-based ECL sensor was further tested and is shown in Fig. 8. The sensor showed little response to non-specific proteins, and no apparent attenuation of ECL intensity was observed upon incubation with non-specific proteins. The strong binding affinity between antigen and antibody was evident in the ultrahigh selectivity of the sensor for CEA.

Table 1 Comparison of the sensitivity responses and limit of detection of different methods and electrode materials for the determination of CEA

Electrode materials	Method	Linear range (ng mL^{-1})	Detection limit (pg mL^{-1})	Ref.
AuNP/BFR/TH	Electrochemical label-free immunosensor	0.025–2	3.5	42
THi-CNTs/AuNPs/Ab_1/HRP-Ab_2-AuNPs-PAN@CNTs	Electrochemical, Sandwich immunosensor	0.02–80	8	43
AuNPs/cysteine/GLD/Ab_1/Ag/Ab_2/Ru-silica@NPG	ECL, Sandwich immunosensor	0.001–10	0.8	44
DMSA-CdTe QDs/Ab_1/Ag/Ab_2/Hemin@NG	ECL, Sandwich immunosensor	0.0001–10	0.024	45
Au-g-C_3N_4 NHs	ECL, label-free immunosensor	0.02–80	6.8	46
AuNPs/(Mn^{2+}-$NaYF_4$:Yb/Er@SiO_2–NH_2)	ECL, label-free immunosensor	0.01–40	5.2	This work

Published on 06 August 2014. Downloaded by University of Illinois at Chicago on 28/10/2014 13:00:31.

Table 2 Assay results of clinical serum samples using the proposed and reference methods (ng mL^{-1})

Sample no.	1	2	3
Proposed method (ECL immunosensor)	26.64	1.88	7.54
Reference method (ELISA)	28.01	1.75	6.93
Relative error (%)	5.10	6.91	8.1

3.6. Using the immunosensor to detect serum tumor markers

In order to evaluate the analytical reliability and feasibility of the immunoassay system for clinical applications, several different stages of cancer patient serum samples were analyzed. The results were compared with those obtained by the ELISA method performed at Nanjing Mingji Hospital. Table 2 shows acceptable results with relative errors ranging from 8.09% to 5.10% for CEA detection, indicating that the ECL immunosensor can provide an alternative tool for protein detection in clinical laboratories.

4. Conclusion

In summary, this study reported the ECL behaviors of Mn^{2+}-doped $NaYF_4$:Yb/Er NPs for the first time. The Mn^{2+} ions disturbed the energy transfer between green and red emissions of Er^{3+} and facilitated the occurrence of red emission, generating a high-intensity ECL signal with sufficient stability. Using SiO_2–NH_2 layers coating $NaYF_4$:Yb/Er NPs and Au NPs that grab the CEA-antibody recognition probe, a novel label-free ECL sensor was fabricated for CEA detection in $K_2S_2O_8$ buffer solution. As an indicator in early-stage cancer and a promising anticancer target for the development of tumor therapeutic agents, measuring the expression level of CEA in the serum of cancer patients is valuable for both clinical diagnosis of cancer in the early stage as well as treatment. The assay results of clinical serum samples were in acceptable agreement with the reference values. The designed immunoassay system possesses ultrahigh sensitivity, satisfactory efficiency, and low toxicity, and might have potentially broad applications in protein diagnostics and bioassays.

Acknowledgements

This work was supported by the Jiangsu Collaborative Innovation Center of Biomedical Functional Materials, National and Local Joint Engineering Research Center of Biomedical Functional Materials, Base of Natural Science Foundation of Jiangsu Province of China (BK 20131396), Natural Science Foundation of Universities of Jiangsu Province (14KJA150006), production, education and research of the prospective joint research project of Jiangsu Province (BY2011109).

References

1 R. Duan, X. Zhou and D. Xing, *Anal. Chem.*, 2010, **82**, 3099.
2 K. A. Fähnrich, M. Pravda and G. G. Guilbault, *Talanta*, 2001, **54**, 531.
3 S. C. B. Gopinath, T. H. Tang, M. Citartan, Y. Chen and T. Lakshmipriya, *Biosens. Bioelectron.*, 2014, **57**, 292–302.
4 P. Khan, D. Idrees, M. A. Moxley, J. A. Corbett, F. Ahmad, G. von Figura, W. S. Sly, A. Waheed and M. I. Hassan, *Appl. Biochem. Biotechnol.*, 2014, **173**, 333–355.
5 S. Deng and H. Ju, *Analyst*, 2013, **138**, 43.
6 J. Wang, *Small*, 2005, **1**, 1036.
7 C. Wang, J. Wu, C. Zong, H. Ju and F. Yan, *Analyst*, 2011, **136**, 4295.
8 Y. Zhang, S. Deng, J. Lei, Q. Xu and H. Ju, *Talanta*, 2011, **85**, 2154.
9 M. Gutierrez-Capitan, A. Ipatov, A. Merlos, C. Jimenez-Jorquera and C. Fernandez-Sanchez, *Electroanalysis*, 2014, **26**, 497–506.
10 S. K. Pasha, A. Kaushik, A. Vasudev, S. A. Snipes and S. Bhansali, *J. Electrochem. Soc.*, 2014, **161**, B3077–B3082.
11 Z. Ding, B. M. Quinn, S. K. Haram, L. E. Pell, B. A. Korgel and A. J. Bard, *Science*, 2002, **296**, 1293.
12 Y. Xu, M. Wu, X. Z. Feng, X. B. Yin, X. W. He and Y. K. Zhang, *Chem.–Eur. J.*, 2013, **19**, 6282.
13 K. Muzyka, *Biosens. Bioelectron.*, 2014, **54**, 393–407.
14 Z. Chen, H. Chen, H. Hu, M. Yu, F. Li, Q. Zhang, Z. Zhou, T. Yi and C. Huang, *J. Am. Chem. Soc.*, 2008, **130**, 3023.
15 S. Watanabe, Y. Hamada, H. Hyodo, K. Soga and M. Matsumoto, *J. Colloid Interface Sci.*, 2014, **422**, 58–64.
16 M. Pokhrel, L. C. Mimun, B. Yust, G. A. Kumar, A. Dhanale, L. Tang and D. K. Sardar, *Nanoscale*, 2014, **6**, 1667–1674.
17 J. J. Zhang, Y. Liu, L. H. Hu, L. P. Jiang and J. J. Zhu, *Chem. Commun.*, 2011, **47**, 6551.
18 M. Yin, L. Wu, Z. Li, J. Ren and X. Qu, *Nanoscale*, 2012, **4**, 400.
19 L. Wu, J. Wang, M. Yin, J. Ren, D. Miyoshi, N. Sugimoto and X. Qu, *Small*, 2014, **10**, 330.
20 S. Watanabe, T. Asanuma, H. Hyodo, K. Soga and M. Matsumoto, *Langmuir*, 2013, **29**, 11185–11191.
21 L. Deng, Y. Shan, J. J. Xu and H. Y. Chen, *Nanoscale*, 2012, **4**, 831.
22 X. F. Wang, J. J. Xu and H. Y. Chen, *J. Phys. Chem. C*, 2008, **112**, 17581.
23 Y. Shan, J. J. Xu and H. Y. Chen, *Chem. Commun.*, 2009, 905–907.
24 G. Tian, Z. Gu, L. Zhou, W. Yin, X. Liu, L. Yan, S. Jin, W. Ren, G. Xing, S. Li and Y. Zhao, *Adv. Mater.*, 2012, **24**, 1226.
25 X. Wang, M. Zhou, Y. Zhu, J. Miao, C. Mao and J. Shen, *J. Mater. Chem. B*, 2013, **1**, 2132.
26 J. Zhang, S. Liu, J. Bao, W. Tu and Z. Dai, *Analyst*, 2013, **138**, 5396.
27 R. Akter, C. K. Rhee and M. A. Rahman, *Biosens. Bioelectron.*, 2014, **54**, 351–357.
28 Z. Altintas and I. Tothill, *Sens. Actuators, B*, 2013, **188**, 988–998.
29 Z. Altintas, S. S. Kallempudi and Y. Gurbuz, *Talanta*, 2014, **118**, 270–276.
30 H. Chon, S. Lee, S. W. Son, C. H. Oh and J. Choo, *Anal. Chem.*, 2009, **81**, 3029.

 This journal is © The Royal Society of Chemistry 2014

Published on 06 August 2014. Downloaded by University of Illinois at Chicago on 28/10/2014 13:00:31.

31 D. Hu, M. Chen, Y. Gao, F. Li and L. Wu, *J. Mater. Chem.*, 2011, **21**, 11276.
32 Z. Li and Y. Zhang, *Angew. Chem., Int. Ed.*, 2006, **118**, 7896.
33 Z. Hou, C. Li, P. a. Ma, Z. Cheng, X. Li, X. Zhang, Y. Dai, D. Yang, H. Lian and J. Lin, *Adv. Funct. Mater.*, 2012, **22**, 2713.
34 Z. Li, L. Wang, Z. Wang, X. Liu and Y. Xiong, *J. Phys. Chem. C*, 2011, **115**, 3291.
35 M. Liu, S. Chen, X. Zhao, Y. Ye, J. Li, Q. Zhu, B. Zhao, W. Zhao, X. Huang and J. Shen, *Talanta*, 2013, **117**, 536.
36 L. L. Li, K. P. Liu, G. H. Yang, C. M. Wang, J. R. Zhang and J. J. Zhu, *Adv. Funct. Mater.*, 2011, **21**, 869.
37 D. Wu, Y. Zhang, L. Shi, Y. Cai, H. Ma, B. Du and Q. Wei, *Electroanalysis*, 2013, **25**, 427.
38 S. A. Zaidi, *Int. J. Electrochem. Sci.*, 2013, **8**, 9936–9955.
39 G. Lai, F. Yan and H. Ju, *Anal. Chem.*, 2009, **81**, 9730.
40 Y. Zhang, H. Chen, X. Gao, Z. Chen and X. Lin, *Biosens. Bioelectron.*, 2012, **35**, 277–283.
41 Z. Song, R. Yuan, Y. Chai, Y. Zhuo, W. Jiang, H. Su, X. Che and J. Li, *Chem. Commun.*, 2010, **46**, 6750.
42 W. B. Lu, C. Qian, L. Y. Bi, L. Tao, J. Ge, J. Dong and W. P. Qian, *Biosens. Bioelectron.*, 2014, **53**, 346.
43 D. X. Feng, L. H. Li, X. Fang, X. W. Han and Y. Z. Zhang, *Electrochim. Acta*, 2014, **127**, 334.
44 M. Zhang, S. G. Ge, W. P. Li, M. Yan, X. R. Song, J. H. Yu, W. Xu and J. D. Huang, *Analyst*, 2012, **137**, 680.
45 S. Y. Deng, J. P. Lei, Y. Huang, Y. Cheng and H. X. Ju, *Anal. Chem.*, 2013, **85**, 5390.
46 L. Chen, X. Zeng, P. Si, Y. Chen, Y. Chi, D. H. Kim and G. Chen, *Anal. Chem.*, 2014, **86**, 4188.